OPEN ACCESS
Journal of Multidisciplinary Applied Natural Science Vol. 5 No. 3 (2025) https://doi.org/10.47352/jmans.2774-3047.283
Check for updates
Research Article

Design of Hydroxyxanthone Derivatives as Breast Cancer Inhibitors: A QSAR Modeling, Molecular Docking, Molecular Dynamics, MM-PBSA and ADMET Prediction

Nela Fatmasari, Faris Hermawan*, Jumina Jumina, Yehezkiel Steven Kurniawan, Harno Dwi Pranowo, Anita Dwi Puspitasari, Lathifah Puji Hastuti, Lala Adetia Marlina, and Nicky Rahmana Putra

Received : March 10, 2025	Revised : July 2, 2025	Accepted : July 16, 2025	Online : July 21, 2025

Abstract
A comprehensive QSAR analysis, in conjunction with molecular docking, molecular dynamics simulations, MM-PBSA binding energy estimations, and ADMET profiling, was conducted to facilitate the development of novel anticancer agents based on hydroxyxanthone derivatives. Molecular and electronic descriptors were calculated using the DFT method with the 3-21G basis set. The best QSAR model identified several descriptors that significantly influence anticancer activity, including the atomic charges at positions C1, C3, C4a, and C7, as well as the highest occupied molecular orbital (HOMO), surface area (SA), molecular volume (VOL), and molecular weight (MW). This model was used to design novel hydroxyxanthone derivatives (X27 to X47). The docking result showed that compounds 7-bromo-3-hydroxy-1-(methylamino)-9*H*-xanthen-9-one (X43), 6-hydroxy-8-(methylamino)-9-oxo-9*H*-xanthene-2-carbonitrile (X44), and 3-hydroxy-7-mercapto-1-(methylamino)-9*H*-xanthen-9-one (X45) had stronger binding energy values than gefitinib as a native ligand. Gefitinib had a binding energy of -6.84 kcal/mol, while those compounds had values of -6.92, -7.12, and -6.92 kcal/mol, respectively. In a molecular dynamics simulation of 100 ns, compounds X43, X44, and X45 exhibited stability comparable to that of gefitinib against the EGFR protein. Additionally, the binding energy MM-PBSA of compound X43 was the lowest (-29.18 kcal/mol), followed by X44 (-27.11 kcal/mol), gefitinib (-26.06 kcal/mol), and X45 (-25.21 kcal/mol). Furthermore, these compounds met Lipinski's rule parameters and the minimal standard parameters in terms of ADMET characteristics, as predicted by physicochemical properties. In conclusion, compounds X43, X44, and X45 are potential anticancer agents for MDA-MB-231 breast cancer cells.

Keywords: QSAR, molecular docking, molecular dynamics, hydroxyxanthone, MM-PBSA, ADMET

1. INTRODUCTION

Cancer remains the leading cause of death globally, responsible for approximately one in six fatalities. As of 2018, the global cancer incidence reached 18.1 million cases, with projections indicating a continued rise to approximately 29.4 million cases by 2040 [1]. Breast cancer is currently the most prevalent cancer worldwide, accounting for 12.5% of all annual new cases [2]. Among the various subtypes of breast cancer, triple-negative breast cancer (TNBC) receives special attention due to its propensity for rapid metastasis [3]. TNBC is a distinct subtype characterized by the absence of estrogen and progesterone receptor expression and lack of HER2 overexpression [4]. Drug therapy remains the conventional approach for the treatment of breast cancer; however, it is associated with numerous adverse effects, including drug resistance, cytotoxicity, and issues related to cost-effectiveness [5]. The limitations of current targeted treatments highlight the need for new therapeutic agents for TNBC. The EGFR overexpression is observed more frequently in TNBC, including MDA-MB-231 and MDA-MB-468, compared to other subtypes of breast cancer [6][7]. The expression of EGFR in human breast tumor tissues is a critical factor in the metastasis and prognosis of breast cancer, particularly in TNBC [8]. Therefore, the EGFR represents a promising target for drug development.

Recent technologies for developing new anticancer agents include computational approaches like quantitative structure-activity relationship (QSAR), molecular docking, and molecular dynamics (MD) simulation [9]-[11]. Those *in silico* studies can reduce time and resources while allowing for the estimation of properties, including toxicity and efficacy, before synthesis [12]. Xanthone derivatives have demonstrated promising anticancer activity across various studies, including *in vitro*, *in vivo*, and clinical trials [13][14]. Xanthone derivatives containing a 3,6-disubstituted

Table 1. Structure and bioactivity of hydroxyxanthones against MDA-MB-231 cancer cells.

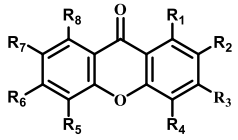

Compound	R_1	R_2	R_3	R_4	R_5	R_6	R_7	R_8	IC_{50} (μM)	pIC_{50}
X1	OH	H	OH	H	H	H	Br	H	0.46	0.34
X2	OH	H	OH	H	H	H	Cl	H	5.20	-0.72
X3*	OH	H	OH	H	H	CH_3	H	H	8.60	-0.93
X4	OCH_3	H	OCH_3	H	H	OH	H	H	9.60	-0.98
X5	OCH_3	H	OCH_3	H	H	H	Cl	H	11.40	-1.06
X6	OH	H	OH	H	H	H	H	H	11.60	-1.06
X7	H	OH	OH	H	H	H	OH	H	23.50	-1.37
X8	H	OH	OH	H	H	OH	H	OH	23.60	-1.37
X9*	OH	H	OH	H	OH	H	H	H	23.80	-1.38
X10	OCH_3	H	OCH_3	H	H	H	H	OH	25.90	-1.41
X11	OH	H	OH	H	H	H	H	OH	33.00	-1.52
X12	H	H	H	OH	H	H	OH	H	43.80	-1.64
X13	H	H	OH	H	H	H	Cl	H	45.60	-1.66
X14*	OH	H	OCH_3	H	H	H	H	OCH_3	34.70	-1.54
X15	H	H	H	OH	H	CH_3	H	H	43.80	-1.64
X16	H	H	OH	H	H	OH	H	H	31.70	-1.50
X17	H	H	OH	H	H	H	OH	H	32.40	-1.51
X18	H	OH	H	H	H	H	OH	H	83.50	-1.92
X19	H	H	H	H	H	H	Br	H	65.90	-1.82
X20*	H	H	OH	OH	H	H	OH	H	53.10	-1.73
X21	OH	H	OH	H	H	H	OH	H	25.10	-1.40
X22	H	H	OH	H	H	H	OCH_3	H	67.10	-1.83
X23	H	H	OH	H	H	OH	H	OH	55.60	-1.75
X24	H	H	H	OH	H	H	Br	H	12.50	-1.10
X25	H	H	H	OH	H	H	Cl	H	57.10	-1.76
X26*	H	H	H	H	H	H	Cl	H	69.40	-1.84

aminocarboxymethoxy moiety showed anticancer activity against the MDA-MB-231 cell line, with an IC_{50} value of 8.06 μM [15]. Several xanthone compounds with a rhamnopyranoside moiety exhibited significant anticancer activity against the MDA-MB-231 cell line, with an IC_{50} value of 4.30 μM [16]. Additionally, benzohydroxyxanthone demonstrated anticancer activity against MDA-MB-231, with an IC_{50} value of 15.8 μM [17]. Adding halogen substituents, including chloro and bromo, to 3,4-dihydroxyxanthone enhanced its anticancer activities against MDA-MB-231 cancer cells [18].

Based on the above findings, a comprehensive evaluation of the relationship between anticancer activity and molecular structure of hydroxyxanthone has not yet been conducted. This study aimed to develop a QSAR model to predict the anticancer activity of hydroxanthone derivatives

against the MDA-MB-231 cell line. The new compounds will be evaluated for their interactions and stability with the EGFR protein using molecular docking and MD simulations. Binding energies will be calculated via molecular mechanics Poisson-Boltzmann surface area (MM-PBSA), and absorption, distribution, metabolism, excretion, and toxicity (ADMET) analysis will assess physicochemical and pharmacokinetic properties.

2. MATERIALS AND METHODS

2.1. Materials

This study utilized an Intel i5-13400 with a VGA GTX 1650 and 32 GB of RAM computer to develop the QSAR equation using 26 hydroxyxanthones [18]. The half-maximal inhibitory concentration (IC_{50}) values against MDA -MB-231 cancer cells were converted to pIC_{50}. As illustrated in Table 1, the dataset is partitioned into two distinct components, i.e., the training set and the test set.

2.2. Methods

2.2.1. QSAR Modelling

The prediction of the proton-nuclear magnetic resonance (^{1}H-NMR) chemical shift for 7-bromo-1,3-dihydroxyxanthone (X1) was conducted utilizing the density functional theory (DFT) method. This analysis employed a basis set comprising STO-3G, 3-21G, and 6-31G. The results were compared with the experimental data. The method demonstrating the lowest correlation error between the experimental and calculated chemical shifts was subsequently selected. The chosen method was also used to calculate descriptors of various hydroxyxanthone derivatives utilizing Gaussian 09 W software [19]. The calculations yielded values for the highest occupied molecular orbital (HOMO), lowest unoccupied molecular orbital (LUMO), and atomic charge (q). The additional descriptors, including surface area (SA), volume (V), partition coefficient (log P), refractivity (MR), polarizability (α), and molecular mass (MW), were calculated utilizing Hyperchem™ version 8.0.10. Furthermore, model validation of QSAR was performed using multiple linear regression analysis utilizing the Build-QSAR program [20]. The selection of the appropriate QSAR model was based on various statistical metrics, including the correlation coefficient (R), the coefficient of determination (R^2), the standard error of estimation (SEE), the ratio of the calculated F value to the tabulated F value (Fcal/Ftab), the sum of squares of predicted residual errors (PRESS), and the cross-validation value (Q^2) [21]. Subsequently, novel xanthone derivatives were designed by considering the descriptors influencing the final QSAR equation and the relationship between the substituents and the pIC_{50} value.

2.2.2. Molecular Docking Study

The preparation of the native ligand and protein was conducted utilizing Chimera [22]. Within Chimera, the standard ligand was selected and inverted across all molecules. Subsequently, all selected molecules were deleted, and the standard ligand was saved in PDB format. Additionally, the protein-ligand complex in the PDB file (3UG2) was cleaned of all residues, including native ligand and water molecules. Subsequently, the protein was saved in the PDB format file. Hydroxyxanthone derivatives were drawn in three-dimensional

Table 2. The ^{1}H NMR chemical shifts by experimental and computational methods (in ppm).

No Atom H	δ Experiment	δ DFT STO-3G	δ DFT 3-21G	δ DFT 6-31G
H2	6.23	7.17	6.65	6.72
H4	6.39	6.48	6.25	6.25
H5	7.63	7.93	7.56	7.49
H6	7.87	8.25	8.04	7.94
H8	8.00	9.01	8.89	8.84
PRESS		2.146	1.022	0.990
R^2		0.827	0.862	0.828

Table 3. QSAR models and statistical parameters.

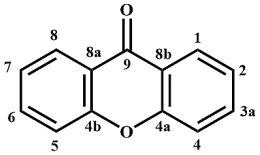

Model	Descriptors	r	r^2	SEE	F	Q^2	PRESS
1	qC8b, qC9, VOL, POL, LogP	0.912	0.832	0.238	14.879	0.634	0.351
2	qC1, qC3, qC4a, qC9, MW, VOL	0.922	0.850	0.233	13.229	0.545	0.405
3	qC1, qC3, qC4a, HOMO, MW, VOL, SA	0.939	0.882	0.215	13.748	0.651	0.639
4	qC1, qC3, qC4a, qC7, VOL, HOMO, SA, MW	0.995	0.912	0.193	15.543	0.675	0.370
5	qC1, qC3, qC4, qC4a, qC8, VOL, HOMO, SA, MR	0.996	0.933	0.175	17.067	0.725	0.355
6	qC1, qC2, qC3, qC4a, qC8, HOMO, SA, LUMO, VOL, MR	0.979	0.958	0.146	22.806	0.751	0.355

structures utilizing GaussView 5.0, and their structures were optimized employing the DFT 3-21G method through Gaussian 09 W. Furthermore, the redocking and docking analyses were conducted utilizing AutoDock4, using a grid box with dimensions of 40×40×40 Å and centered at the coordinates 0.26, 48.42, and 21.15 for the x, y, and z axes, respectively [23]. A total of 50 docking runs were carried out using the Lamarckian Genetic Algorithm (LGA). The docking results were visualized using Discovery Studio Visualizer [24] [25].

2.2.3. MD Simulation and Calculation of MM-PBSA Energy

The MD simulations were conducted using the GROMACS 2023 software [26][27]. The topology for the EGFR protein was created using the CHARMM36 force field [28]. The topology parameters for all ligands were generated with the aid of the cgenff server (cgenff.com) [27]. Periodic boundary conditions (PBC) were implemented to create a simplified representation of the actual system. Energy minimization was conducted using the steepest descent method for a duration of 1 ns, with the process concluding once the energy reached a threshold of 10 kJ/mol. Subsequently, equilibration was performed utilizing both the NVT and NPT ensembles, each sustained for 1 ns with a time step of 2 fs, under conditions of 300 K and 1 atm. The system parameters were maintained isotropically, and long-range electrostatic interactions were addressed using the Particle Mesh Ewald (PME) method. Additionally, temperature coupling was achieved through a modified Berendsen thermostat employing the v-rescale technique [29]-[31]. The MD simulations of hydroxyxanthones targeting the EGFR receptor were conducted for 100 ns under consistent conditions. The outcomes of the MD simulation included analyses of root mean square deviation (RMSD), root mean square fluctuation (RMSF), radius of gyration (Rg), and hydrogen bond (H-bond) interactions. Furthermore, the calculation of free binding energies was performed utilizing the g_mmpbsa program, as described by Kumari et al. [32]. The MD trajectory data for the ligand-protein complex and the associated parameter file were employed to perform a single-step calculation within the g_mmpbsa framework.

2.2.4. ADMET Prediction

The structures of hydroxyxanthone derivatives in PDB format were converted to SMILES format utilizing Discovery Studio Visualizer. Subsequently, these structures were submitted individually to the pkCSM web server [33]. The selection of physicochemical and ADMET parameters was performed using the ADMET menu. Following this, the pkCSM server provided detailed data for each compound, encompassing Lipinski's Rule of Five, as well as parameters

related to adsorption, distribution, metabolism, excretion, and toxicity.

3. RESULTS AND DISCUSSIONS

3.1. QSAR Modeling

A comparison of ^{1}H-NMR chemical shifts between experimental data and computational predictions is presented in Table 2. The computational results were obtained using the DFT method with a basis set comprising STO-3G, 3-21G, and 6-31G. The results indicated that the DFT method with the 3-21G basis set produced the highest R^2 (0.8621). This approach leads to enhanced accuracy in predicting both the geometry and properties of molecules when compared to minimal basis sets such as STO-3G, which do not possess the same level of flexibility [34]. The QSAR model relies on the availability of activity data sets obtained from wet laboratory experiments. This model facilitates the comparison between the chemical structure of a compound and its biological activity [35]. Subsequently, selecting the best QSAR model required a thorough evaluation of various statistical parameters to ensure its validity and predictive efficacy. The BuildQSAR software with the Genetic Algorithm (GA) method successfully generated six predictive QSAR models, which were subsequently validated through various statistical parameters (Table 3). A well-established QSAR model was defined by a R^2 value of 0.6 or greater and a Q^2 value that surpasses 0.5 [36].

As shown in Table 3, all QSAR models fulfill the requirements for the coefficient of determination and the cross-validated coefficient. Subsequently, six QSAR models were subjected to external validity testing to evaluate their capacity to predict anticancer activity within the test set. The purpose of this validation process was to evaluate whether the six QSAR models fulfill the statistical criteria necessary for accurately predicting anticancer activity in datasets that differ from the training set [37].

According to the R^2 and PRESS value for the test set, model 4 demonstrated the highest R^2 and the lowest PRESS value (Table 4). A more robust QSAR model is indicated by a coefficient of determination approaching 1.0 [36]. As a result, model 4 was regarded as the most effective model among those assessed. The QSAR equation of model 4 was pIC_{50} = (+1.874*qC1) + (2.069*qC3) - (31.869*qC4a) - (0.704*qC7) + (39.315*HOMO) + (0.064*SA) - (0.057*VOL) + (0.023*MW) + (27.243).

3.2. Design of New Xanthone Derivatives

Based on the best QSAR equation (model 4), increasing HOMO, MW, SA, qC1, and qC3 could increase anticancer activity. However, increasing VOL, qC4a, and qC7 would decrease cytotoxic activity. To enhance cytotoxic activity, we added electron-donating groups (EDGs) such as sulfur (S) and amino groups (NH_2) and electron-withdrawing groups (EWGs) such as F and CF_3 to our new design compound. The EDGs, such as S and NH_2, significantly influence the energy levels of the HOMO in xanthone derivatives, which is crucial for their cytotoxic effects [38]. Meanwhile, the EWGs like F, Br, and CF_3 alter the electronic distribution within the xanthone structure. These groups can stabilize the electron-deficient areas of the

Table 4. Comparison of the experimental pIC_{50} with the predicted pIC_{50} in the test set.

Test set	pIC_{50} experiment	pIC_{50} prediction					
		Model 1	Model 2	Model 3	Model 4	Model 5	Model 6
3	-0.934	-0.752	-1.131	-1.140	-0.896	-0.985	-0.854
9	-1.377	-0.784	-0.936	-1.332	-1.275	-1.888	-1.984
14	-1.540	-1.100	-1.514	-1.369	-1.287	-0.826	-0.963
20	-1.725	-1.141	-1.041	-1.432	-1.749	-2.481	-2.278
26	-1.841	-2.078	-2.315	-2.623	-2.653	-2.598	-2.814
PRESS		0.975	0.925	0.771	0.734	1.916	1.959
R^2 Prediction		0.589	0.310	0.497	0.726	0.509	0.598

Table 5. The novel hydroxyxanthones were obtained from the best QSAR model.

Compound	R_1	R_2	R_3	R_4	R_5	R_6	R_7	R_8	IC_{50} (prediction)
X27	OH	H	OH	H	H	H	F	H	6.942
X28	OH	H	OH	H	H	H	CF_3	H	2.617
X29	OH	H	OH	H	H	H	SH	H	6.059
X30	OH	H	OH	H	H	H	SO_3H	H	5.131
X31	OH	H	OH	H	H	H	CN	H	7.243
X32	NH_2	H	OH	H	H	H	H	H	0.799
X33	NH_2	H	OH	H	H	H	F	H	6.441
X34	NH_2	H	OH	H	H	H	Cl	H	4.171
X35	NH_2	H	OH	H	H	H	Br	H	0.888
X36	NH_2	H	OH	H	H	H	CN	H	3.002
X37	NH_2	H	OH	H	H	H	SH	H	8.496
X38	NH_2	H	OH	H	H	H	SO_3H	H	1.799
X39	NH_2	H	OH	H	H	H	CF_3	H	2.174
X40	$NH(CH_3)$	H	OH	H	H	H	H	H	1.321
X41	$NH(CH_3)$	H	OH	H	H	H	F	H	1.132
X42	$NH(CH_3)$	H	OH	H	H	H	Cl	H	0.705
X43	$NH(CH_3)$	H	OH	H	H	H	Br	H	0.161
X44	$NH(CH_3)$	H	OH	H	H	H	CN	H	0.420
X45	$NH(CH_3)$	H	OH	H	H	H	SH	H	1.350
X46	$NH(CH_3)$	H	OH	H	H	H	SO_3H	H	0.309
X47	$NH(CH_3)$	H	OH	H	H	H	CF_3	H	0.393

molecule, enhancing interactions with biological targets such as enzymes and receptors involved in cancer cell proliferation and survival [39]. Specifically, they can influence the reactivity of the xanthone's aromatic system, making it more favorable for interactions that lead to cytotoxic effects. The newly developed hydroxyxanthone derivatives, designated as X27 to X47, are presented in Table 5.

3.3. Molecular Docking Study

Hydroxyxanthone compounds identified through QSAR analysis with predicted IC_{50} values below 2 µM were further subjected to molecular docking studies to evaluate their interactions with the EGFR protein. Our research highlights hydroxyxanthones as potential anti-cancer leads and emphasizes the importance of gefitinib's therapeutic benchmark in guiding drug design [40][41]. The redocking analysis found that gefitinib has a binding energy of -6.84 kcal/mol and an RMSD value of 1.59 Å. The RMSD values, which are indicative of the accuracy of the docking, constantly remained below 2 Å [42]. Molecular docking analysis demonstrated that the binding energies of X32, X35, and X38–X47 ranged from -5.67 to -7.12 kcal/mol. Among these, compounds X43, X44, and X45 exhibited significantly more negative binding energy values than the native ligand, gefitinib, indicating a potentially stronger binding affinity to the EGFR protein. Gefitinib had a binding energy of -6.84 kcal/mol, while X43, X44, and X45 exhibited values of -6.92, -7.12, and -6.92 kcal/mol, respectively (Table 6). A more negative binding energy suggests a stronger affinity for the target receptor's active site, implying that X43, X44, and X45 may be more effective inhibitors than gefitinib [43].

As shown in Figure 1, gefitinib formed a H-bond with Met793 and various non-covalent interactions, including alkyl, sigma, halogen, and a salt-bridge with key amino acids like Leu718, Val726, Ala743,

Leu788, Met790, Asp800, and Leu844. In contrast, compounds X43, X44, and X45 also formed H-bonds with Met793, but notably, they formed more H-bonds overall. For instance, X44 and X45 had additional H-bonds with Leu718, Ser719, and Gln791, while X43 maintained a similar interaction pattern with increased hydrogen binding interactions compared to gefitinib. The higher number of H-bonds found in the complexes with X43, X44, and X45 suggested an enhanced stability of these ligand-receptor interactions. Hydrogen bonding is generally a stronger interaction and more stable than other non-covalent interactions such as pi-alkyl, pi-sigma [44], or halogen bonding, strengthening the ligand binding [45][46]. Consequently, the increased inhibition efficiency of X43, X44, and X45 compared to gefitinib can be attributed to better binding energy and increased stabilizing H-bonds. Compounds X43, X44, and X45, which exhibited lower binding energies compared to the other hydroxyxanthones and formed H-bond interactions analogous to those observed with gefitinib, were subsequently analyzed for complex stability through MD simulations.

3.4. MD Simulation

The RMSD plot evaluated the stability of different ligands (X43, X44, X45, and gefitinib) bound to the target protein over a 100-ns MD simulation (Figure 2). A RMSD value represents the average displacement of the atomic positions of a system relative to an initial reference structure. A lower RMSD value indicates that the system remains close to the initial position, suggesting more excellent structural stability. The RMSD values of all ligands range from 0.5 to 2.0 Å (Figure 2(a)), suggesting minimal fluctuations within the protein's active site and stable ligand–protein interactions throughout the 100 ns simulation. As illustrated in Figure 2(b), RMSD analysis of the ligand-protein backbone complexes revealed that gefitinib exhibited higher RMSD values, indicating lower structural stability compared to compounds X43, X44, and X45. The relatively stable RMSD profiles of X43, X44, and X45 suggest stronger and more consistent interactions with the binding site, leading to reduced conformational fluctuations during the simulation [47]. These findings were consistent with the previous docking binding energy studies, which showed that ligands X43, X44, and X45 had higher stable affinities than the other ligands. These findings provided a solid foundation for considering X43, X44, and X45 as more promising candidates. Overall, these comparisons provide insight into the tested ligands' differential binding stability and conformational dynamics, which can be valuable for guiding ligand selection and further optimization [48].

The RMSF plot provided insight into the residue flexibility of the protein backbone for complexes bound with X43, X44, X45, and gefitinib (Figure 3

Table 6. Molecular docking results of compounds X32, X35, X38-X47, and gefitinib.

Compound	Binding Energy	Interactions
X32	-5.88	Leu718, Ser719, Met793, Leu844
X35	-6.50	Leu718, Val726, Met739, Ala743, Cys775
X38	-5.67	Ala743, Met793, Pro794, Leu844, Thr854
X40	-6.40	Leu718, Ser719, Val726, Ala743, Met793, Leu844
X41	-6.23	Ser719, Val726, Ala743, Met793, Leu844
X42	-6.67	Leu718, Ser719, Val726, Ala743, Met793, Leu844
X43	-6.92	Leu718, Val726, Ala743, Met793, Leu844
X44	-7.12	Leu718, Ser719, Val726, Ala743, Gln791, Met793, Leu844
X45	-6.92	Leu718, Ser719, Val726, Ala743, Gln791, Met793, Leu844
X46	-6.03	Val726, Ala743, Met790, Gln791, Met793, Leu844
X47	-6.06	Leu718, Val726, Ala743, Arg776, Met790, Gln791, Met793, Leu844
Gefitinib	-6.84	Leu718, Val726, Ala743, Leu788, Met790, Met793, Aps800, Leu844

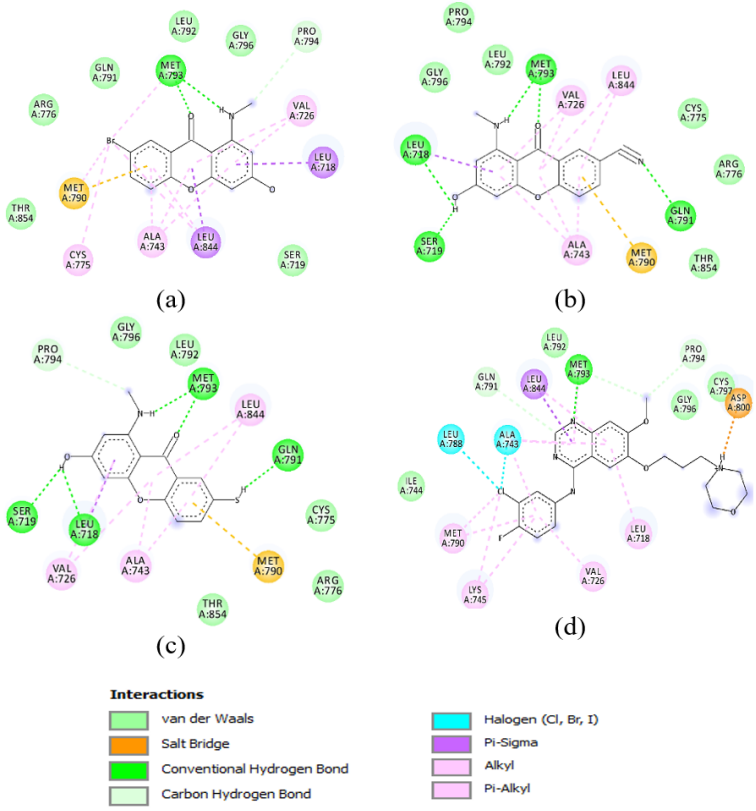

Figure 1. The visualization of intermolecular interactions of compounds (a) X43, (b) X44, (c) X45, and (d) gefitinib.

(a)). Molecular docking results demonstrated that ligand-protein interactions predominantly occur within the amino acid residue range of 700–850, with all ligands forming H-bonds specifically at Met793. Correspondingly, the RMSF analysis revealed minimal atomic fluctuations in this region, indicating stable ligand binding at Met793 and underscoring its critical role in the structural integrity of the EGFR binding site. Compounds X43, X44, and X45, RMSF profiles appeared primarily similar, with only localized differences in certain regions. This similarity suggested that, in general, the binding of X43, X44, X45, or gefitinib does not drastically alter the global dynamics of the protein. However, the pronounced fluctuation in the region above residue 900 may imply unique ligand-induced conformational changes that could affect binding affinity or the protein's functional mechanisms [49].

The Rg plot that was illustrated in Figure 3(b) showed that all complexes exhibit relatively similar Rg values, suggesting that the protein maintains a compact and stable structure. However, as the simulation progresses, subtle differences become evident, with the gefitinib-bound complex often displaying slightly higher Rg values than those bound with the X43, X44, and X45 ligands. This pattern indicated that the protein complexed with gefitinib may adopt a less compact or more expanded conformation, possibly due to weaker binding or more flexible rearrangements. In contrast, complexes with X43, X44, and X45 exhibited lower and more stable Rg values, implying more compact and more stabilizing ligand interactions. Their relatively consistent Rg profiles suggested these ligands induce or maintain a more stable protein structure pack over the simulation. The number of H-bonds shown in Figure 4 indicates how consistently each ligand forms H-bonds to the EGFR protein during the simulation. The X45 complex showed relatively stable H-bond interactions due to the formation of two H-bonds during the simulation time [50]. This consistent interaction suggested a strong and steady ligand-protein association that may enhance overall stability. Meanwhile, X43 and X44 formed H-bonds. However, fluctuates between one and three H-bonds throughout the simulation time. In

contrast, gefitinib showed a pattern of fewer and more variable H-bonds, rarely stabilizing above one H-bond at any given time.

3.5. MM-PBSA Binding Energy

The MM-PBSA results comprehensively break down the intermolecular interactions and their contributions to the overall binding affinity of the tested ligands (X43, X44, X45, and gefitinib) for the target protein [51]. Each energy component, van der Waals, electrostatic, polar solvation, and nonpolar solvation, is critical in shaping the final binding energy [52]. As shown in Table 7, compound X43 exhibited the lowest binding energy (-29.18 kcal/mol), followed by X44 (-27.11 kcal/mol), gefitinib (-26.06 kcal/mol), and X45 (-25.21 kcal/mol). Focusing on the energy component, X43 showed strong binding affinity through van der Waals interactions (-33.89 kcal/mol). These observations highlight that while strong gas-phase interaction (van der Waals) is crucial, the ultimate determinant of binding affinity often depends on how these interactions are balanced against the solvation factors [53].

3.6. Pharmacokinetic Properties and Lipinski's Rule

The prediction of physicochemical and ADMET properties plays a critical role in the drug discovery process. This assessment is vital for evaluating the potential of small-molecule drugs in terms of their metabolism, distribution, absorption, efficacy, and safety profiles. This approach avoids investing time in toxic lead compounds, which may become metabolically inactive or fail to pass through biological membranes [54]. According to Lipinski's Rule of Five, an ideal drug candidate should meet the following criteria: molecular weight of less than 500 Da, a logarithm of the octanol-water partition coefficient (log P) of less than 5, fewer than 10 rotatable bonds, fewer than 10 H-bond acceptors, fewer than 5 H-bond donors, and a polar surface area of less than 140 Å [55]. As demonstrated in Table 8, all compounds (X43, X44, and X45) adhere to the parameters established by the Lipinski rule of five.

Regarding absorption, all three compounds had good CaCo2 permeability values (around 1.05 to 1.09), suggesting that they can be efficiently absorbed via the intestinal epithelium (Table 8). Their intestinal absorption values were also notably high, exceeding 92% in all cases. The skin

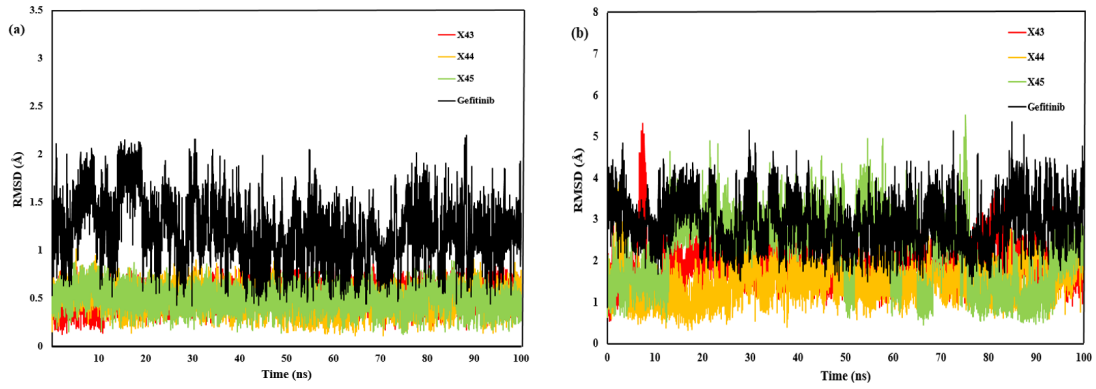

Figure 2. RMSD graphs of (a) ligands and (b) ligand-EGFR complexes.

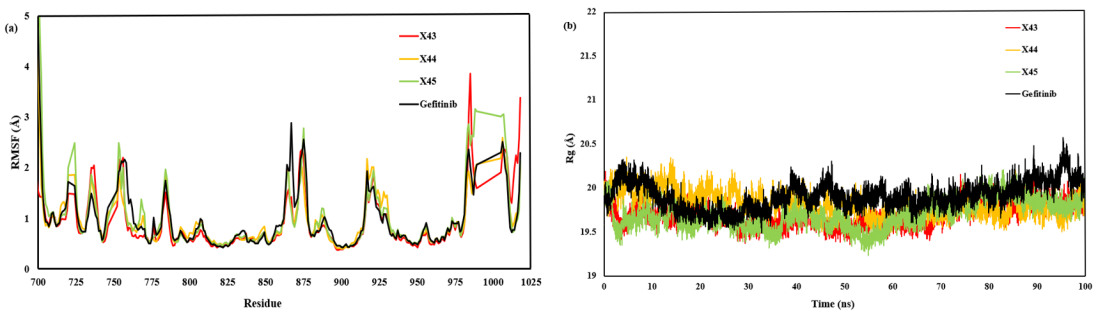

Figure 3. (a) The RMSF and (b) radius of gyration of X43, X44, X45, and gefitinib.

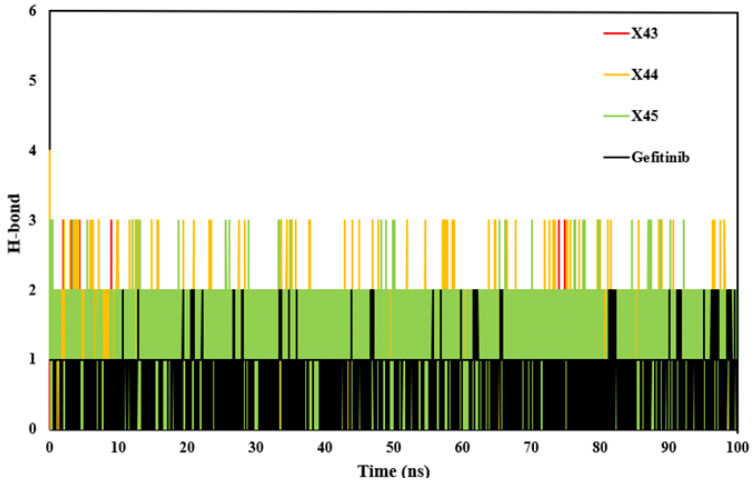

Figure 4. Hydrogen bond of X43, X44, X45, and gefitinib.

Table 7. MM-PBSA binding energy of X43, X44, X45, and gefitinib.

Compound	van der Waal's energy	Electrostatic energy	Polar solvation energy	Nonpolar solvation energy	Gas-phase free energy	Solvation free energy	Binding energy (kcal/mol)
X43	-33.89	-6.17	14.10	-3.21	-40.07	10.89	-29.18
X44	-31.22	-13.29	20.74	-3.34	-44.51	17.40	-27.11
X45	-31.02	-9.10	18.14	-3.24	-40.11	14.90	-25.21
Gefitinib	-33.74	-9.62	21.66	-4.36	-43.37	17.31	-26.06

permeability values were very similar and opposed, indicating relatively low transdermal absorption [56]. The volume of distribution (VDss) was slightly negative for X45 (-0.149), suggesting a tendency to remain in plasma or a lower tissue distribution compared to X43 (0.027) and X44 (0.046). When considering blood-brain barrier (BBB) permeability, all three compounds exhibited modest but positive values (0.134 for X43 and 0.169 for X45), implying they can potentially cross into the CNS to some extent; their CNS permeability values were negative and quite similar (in a range of -1.9 to -2.1), indicating limited brain penetration despite some BBB permeability.

The metabolism characteristics showed that none of the three compounds were unsuitable as CYP2D6 and CYP3A4 substrates. Notably, X44 and X45 were predicted to be CYP3A4 inhibitors. Regarding excretion, total clearance values for the three compounds were on a similar scale (0.330 to 0.507), suggesting moderate elimination rates. Subsequently, none were indicated as renal OCT2 substrates. Finally, toxicity predictions showed no significant alerts for AMES toxicity and hERG I inhibition, which are critical toxicity endpoints. The maximum tolerated dose values for compounds X43, X44, and X45 were 0.606, 0.498, and 0.801, respectively. While none were predicted to be hERG I inhibitors. Compounds X43, X44, and X45 appeared to have no hepatotoxicity potential and showed no skin sensitization issues.

4. CONCLUSIONS

The most suitable QSAR model had been found as pIC_{50} = (+1.874*qC1) + (2.069*qC3) - (31.869*qC4a) - (0.704*qC7) + (39.315*HOMO) + (0.064*SA) - (0.057*VOL) + (0.023*MW) + (27.243). This model was used to design novel hydroxyxanthones (X27 to X47). Molecular docking results showed that three hydroxyxanthones (X43, X44, and X45) demonstrated outstanding inhibitory action for the EGFR protein. The 100 ns MD simulation demonstrated that compounds X43, X44, and X45 had EGFR stability comparable to gefitinib.

Meanwhile, the MM-PBSA binding energy of compounds X43 and X44 was lower than gefitinib. According to the prediction of physicochemical properties, molecules X43, X44, and X45 meet the requirements of Lipinski's rule, the minimal standard parameters in ADMET characteristics. In summary, compounds X43, X44, and X45 are promising candidates for new anticancer agents. The results of this study provide a foundational basis for subsequent investigations, including the chemical synthesis of compounds X43, X44, and X45, followed by *in vitro* evaluation of their anticancer efficacy against MDA-MB-231 breast cancer cell lines.

AUTHOR INFORMATION

Corresponding Author

Faris Hermawan — Research Center for Pharmaceutical Ingredient and Traditional Medicine, National Research and Innovation Agency (BRIN), Tangerang Selatan-15314 (Indonesia);

orcid.org/0009-0006-6923-4050

Email: fari025@brin.go.id

Authors

Nela Fatmasari — Department of Chemistry Education, Sultan Ageng Tirtayasa University, Serang-42117 (Indonesia);

orcid.org/0000-0003-0376-8923

Table 8. Physicochemical and ADMET properties of compounds X43, X44, and X45.

Properties		Compound		
		X43	X44	X45
Physicochemical	Molecular weight	320.142	266.256	273.313
	log P	3.456	2.565	2.982
	Rotatable bond	1	1	1
	H-bond acceptor	4	5	5
	H-bond donor	2	2	3
	Surface area	116.338	113.228	113.625
Absorption	$CaCO_2$ permeability	1.051	1.092	1.091
	Intestinal absorption	92.962	95.487	92.476
	Skin permeability	-2.737	-2.737	-2.735
Distribution	VDss	0.027	0.046	-0.149
	BBB permeability	0.134	-0.203	0.169
	CNS permeability	-1.915	-2.106	-2.017
Metabolism	CYP2D6 substrate	No	No	No
	CYP3A4 substrate	No	No	No
	CYP2D6 inhibitor	No	No	No
	CYP3A4 inhibitor	No	Yes	Yes
Excretion	Total clearance	0.330	0.507	0.338
	Renal OCT2 substrate	No	No	No
Toxicity	AMES Toxicity	Yes	Yes	Yes
	Max. Tolerated dose	0.606	0.498	0.801
	hERG I inhibitor	No	No	No
	hERG II inhibitor	Yes	Yes	Yes
	Hepatoxicity	No	No	No
	Skin sensitization	No	No	No

Jumina Jumina — Department of Chemistry, Universitas Gadjah Mada, Yogyakarta-55281 (Indonesia);
orcid.org/0000-0003-2604-7838
Yehezkiel Steven Kurniawan — Department of Chemistry, Universitas Gadjah Mada, Yogyakarta-55281 (Indonesia);
orcid.org/0000-0002-4547-239X
Harno Dwi Pranowo — Department of Chemistry, Universitas Gadjah Mada, Yogyakarta-55281 (Indonesia); Austrian-Indonesian Centre (AIC) for Computational Chemistry, Department of Chemistry, Universitas Gadjah Mada, Yogyakarta-55281 (Indonesia);
orcid.org/0000-0002-0223-5036
Anita Dwi Puspitasari — Faculty of Pharmacy, Universitas Wahid Hasyim, Semarang-50236 (Indonesia);
orcid.org/0000-0001-7779-2702
Lathifah Puji Hastuti — Graduate School, Universitas Padjadjaran, Bandung-45363 (Indonesia);
orcid.org/0000-0002-4976-4218
Lala Adetia Marlina — Research Center for Computing, National Research and Innovation Agency (BRIN), Bogor-16911 (Indonesia);
orcid.org/0009-0000-9313-9850
Nicky Rahmana Putra — Research Center for Pharmaceutical Ingredient and Traditional Medicine, National Research and Innovation Agency (BRIN), Tangerang Selatan-15314 (Indonesia);
orcid.org/0000-0003-4886-496X

Author Contributions

F. H. and N. F. were responsible for the development and design of the research concept. L. A. M. and H. D. P. focused on optimizing the structure of hydroxyxanthone derivatives utilizing the density functional theory (DFT) method. Subsequently, A. D. P. conducted a quantitative structure-activity relationship (QSAR) analysis, from which J. J. and N. R. P. designed novel hydroxyxanthone derivatives based on the most efficient QSAR model. Y. S. K. executed a molecular docking study targeting the epidermal growth factor receptor (EGFR) protein. In addition, F. H. performed a 100-ns molecular dynamics simulation and calculated the binding energy of hydroxyxanthone derivatives against the EGFR protein using the MM-PBSA method. Finally, L. P. H. successfully predicted the compounds' absorption, distribution, metabolism, excretion, and toxicity (ADMET) characteristics.

Conflicts of Interest

The authors declare no conflict of interest.

ACKNOWLEDGEMENT

The authors express their gratitude to the Austrian-Indonesian Center for Computational Chemistry (AIC), Department of Chemistry, Faculty of Mathematics and Natural Sciences, Universitas Gadjah Mada, for providing licenses for Gaussian09 and Hyperchem, which facilitated the theoretical studies conducted in this research.

REFERENCES

[1] R. L. Siegel, K. D. Miller, H. E. Fuchs, and A. Jemal. (2022). "Cancer statistics, 2022". *CA: A Cancer Journal for Clinicians.* **72** (1): 7-33. 10.3322/caac.21708.

[2] R. Dolatkhah, M. H. Somi, M. A. Jafarabadi, M. Hosseinalifam, S. Sepahi, M. Belalzadeh, M. Nezamdoust, and S. Dastgiri. (2020). "Breast Cancer Survival and Incidence: 10 Years Cancer Registry Data in the Northwest, Iran". *International Journal of Breast Cancer.* **2020** : 1963814. 10.1155/2020/1963814.

[3] K. Hu, J. H. Law, A. Fotovati, and S. E. Dunn. (2012). "Small interfering RNA library screen identified polo-like kinase-1 (PLK1) as a potential therapeutic target for breast cancer that uniquely eliminates tumor-initiating cells". *Breast Cancer Research.* **14** (1): R22. 10.1186/bcr3107.

[4] G. Palma, G. Frasci, A. Chirico, E. Esposito, C. Siani, C. Saturnino, C. Arra, G. Ciliberto, A. Giordano, and M. D'Aiuto. (2015). "Triple negative breast cancer: looking for the missing link between biology and treatments". *Oncotarget.* **6** (29): 26560-74. 10.18632/oncotarget.5306.

[5] P. De Cicco, M. V. Catani, V. Gasperi, M. Sibilano, M. Quaglietta, and I. Savini. (2019). "Nutrition and Breast Cancer: A Literature Review on Prevention, Treatment and Recurrence". *Nutrients.* **11** (7). 10.3390/nu11071514.

[6] Y. S. Kurniawan, H. Amrulloh, E. Yudha, N. Fatmasari, F. Hermawan, A. Fitria, H. D. Pranowo, E. N. Sholikhah, and J. Jumina. (2024). "Evaluation of Xanthone and Cinnamoylbenzene as Anticancer Agents for Breast Cancer Cell Lines through In Vitro and In Silico Assays". *Journal of Multidisciplinary Applied Natural Science.* **5** (1): 87-102. 10.47352/jmans.2774-3047.231.

[7] C. Lefebvre and A. L. Allan. (2021). "Anti-proliferative and anti-migratory effects of EGFR and c-Met tyrosine kinase inhibitors in triple negative breast cancer cells". *Precision Cancer Medicine.* **4** : 2-2. 10.21037/pcm-20-62.

[8] R. H. Li, W. H. Huang, J. D. Wu, C. W. Du, and G. J. Zhang. (2017). "EGFR expression is associated with cytoplasmic staining of CXCR4 and predicts poor prognosis in triple-negative breast carcinomas". *Oncology Letters.* **13** (2): 695-703. 10.3892/ol.2016.5489.

[9] J. Verma, V. M. Khedkar, and E. C. Coutinho. (2010). "3D-QSAR in drug design--a review". *Current Topics in Medicinal Chemistry.* **10** (1): 95-115. 10.2174/156802610790232260.

[10] Y. S. Kurniawan, N. Fatmasari, J. Jumina, H. D. Pranowo, and E. N. Sholikhah. (2023). "Evaluation of The Anticancer Activity of Hydroxyxanthones Against Human Liver Carcinoma Cell Line". *Journal of Multidisciplinary Applied Natural Science.* **4** (1): 1-15. 10.47352/jmans.2774-3047.165.

[11] M. S. Badar, S. Shamsi, J. Ahmed, and M. A. Alam. (2022). In: "Transdisciplinarity, (Integrated Science, ch. Chapter 7". 131-151. 10.1007/978-3-030-94651-7_7.

[12] S. H. Abdullahi, A. Uzairu, G. A. Shallangwa, S. Uba, and A. B. Umar. (2022). "In-silico activity prediction, structure-based drug design, molecular docking and pharmacokinetic studies of selected quinazoline derivatives for their antiproliferative activity against triple negative breast cancer (MDA-MB231) cell line". *Bulletin of the National Research Centre.* **46** (1). 10.1186/s42269-021-00690-z.

[13] Y. S. Kurniawan, K. T. A. Priyangga, Jumina, H. D. Pranowo, E. N. Sholikhah, A. K. Zulkarnain, H. A. Fatimi, and J. Julianus. (2021). "An Update on the Anticancer Activity of Xanthone Derivatives: A Review". *Pharmaceuticals (Basel).* **14** (11). 10.3390/ph14111144.

[14] Q. G. Su, Y. Liu, Y. C. Cai, Y. L. Sun, B. Wang, and L. J. Xian. (2011). "Anti-tumour effects of xanthone derivatives and the possible mechanisms of action". *Investigational New Drugs.* **29** (6): 1230-40. 10.1007/s10637-010-9468-5.

[15] C. Liu, M. Zhang, Z. Zhang, S. B. Zhang, S. Yang, A. Zhang, L. Yin, S. Swarts, S. Vidyasagar, L. Zhang, and P. Okunieff. (2016). "Synthesis and anticancer potential of novel xanthone derivatives with 3,6-substituted chains". *Bioorganic & Medicinal Chemistry.* **24** (18): 4263-4271. 10.1016/j.bmc.2016.07.020.

[16] G.-p. Song, S.-m. Li, H.-z. Si, Y.-b. Li, Y.-s. Li, J.-h. Fan, Q.-q. Liang, H.-b. He, H.-m. Ye, and Z.-n. Cui. (2015). "Synthesis and bioactivity of novel xanthone and thioxanthone l-rhamnopyranosides". *RSC Advances.* **5** (45): 36092-36103. 10.1039/c5ra02846a.

[17] P. Cheng, L. Zhu, W. Guo, W. Liu, J. Yao, G. Dong, Y. Zhang, C. Zhuang, C. Sheng, Z. Miao, and W. Zhang. (2012). "Synthesis of novel benzoxanthone analogues as non-Camptothecin topoisomerase I inhibitors". *Journal of Enzyme Inhibition and Medicinal Chemistry.* **27** (3): 437-42. 10.3109/14756366.2011.595712.

[18] J. Liu, J. Zhang, H. Wang, Z. Liu, C. Zhang, Z. Jiang, and H. Chen. (2017). "Synthesis of xanthone derivatives and studies on the inhibition against cancer cells growth and synergistic combinations of them". *European Journal of Medicinal Chemistry.* **133** : 50-61. 10.1016/j.ejmech.2017.03.068.

[19] M. J. Frisch, G. W. Trucks, H. B. Schlegel, G. E. Scuseria, M. A. Robb, J. R. Cheeseman, G. Scalmani, V. Barone, B. Mennucci, G. A. Petersson, H. Nakatsuji, M. Caricato, X. Li, H. P. Hratchian, A. F. Izmaylov, J. Bloino, G. Zheng, J. L. Sonnenberg, M. Hada, M. Ehara, K. Toyota, R. Fukuda, J. Hasegawa, M. Ishida, T. Nakajima, Y. Honda, O. Kitao, H. Nakai, T. Vreven, J. A. J. Montgomery, J. E. Peralta, F. Ogliaro, M. Bearpark, J. J. Heyd, E. Brothers, K. N. Kudin, V. N. Staroverov, R. Kobayashi, J. Normand, K. Raghavachari, A. Rendell, J. C. Burant, S. S. Iyengar, J. Tomasi, M. Cossi, N. Rega, J. M. Millam, M. Klene, J. E. Knox, J. B. Cross, V. Bakken, C. Adamo, J. Jaramillo, R. Gomperts, R. E. Stratmann, O. Yazyev, A. J. Austin, R. Cammi, C. Pomelli, J. W. Ochterski, R. L. Martin, K. Morokuma, V. G. Zakrzewski, G. A. Voth, P. Salvador, J. J. Dannenberg, S. Dapprich, A. D. Daniels, O. Farkas, J. B. Foresman, J. V. Ortiz, J. Cioslowski, and D. Fox.(2013). "Gaussian-09 Revision D.01". Wallingford CT: Gaussian Inc.

[20] D. B. de Oliveira and A. C. Gaudio. (2000). "BuildQSAR: A New Computer Program for QSAR Analysis". *Quantitative Structure-Activity Relationships.* **19** (6): 599-601. 10.1002/1521-3838(200012)19:6<599::Aid-qsar599>3.0.Co;2-b.

[21] S. Shayanfar and A. Shayanfar. (2022). "Comparison of various methods for validity evaluation of QSAR models". *BMC Chemistry.* **16** (1): 63. 10.1186/s13065-022-00856-4.

[22] E. F. Pettersen, T. D. Goddard, C. C. Huang, G. S. Couch, D. M. Greenblatt, E. C. Meng, and T. E. Ferrin. (2004). "UCSF Chimera--a visualization system for exploratory research and analysis". *Journal of Computational Chemistry.* **25** (13): 1605-12. 10.1002/jcc.20084.

[23] G. M. Morris, R. Huey, W. Lindstrom, M. F. Sanner, R. K. Belew, D. S. Goodsell, and A. J. Olson. (2009). "AutoDock4 and AutoDockTools4: Automated docking with selective receptor flexibility". *Journal of Computational Chemistry.* **30** (16): 2785-91. 10.1002/jcc.21256.

[24] J. Fuhrmann, A. Rurainski, H. P. Lenhof, and D. Neumann. (2010). "A new Lamarckian genetic algorithm for flexible ligand-receptor docking". *Journal of Computational Chemistry.* **31** (9): 1911-8. 10.1002/jcc.21478.

[25] D. S. Biovia.(2019). "Discovery Studio Visualizer". San Diego.

[26] B. Hess, C. Kutzner, D. van der Spoel, and E. Lindahl. (2008). "GROMACS 4: Algorithms for Highly Efficient, Load-Balanced, and Scalable Molecular Simulation". *Journal of Chemical Theory and Computation.* **4** (3): 435-47. 10.1021/ct700301q.

[27] S. Pronk, S. Pall, R. Schulz, P. Larsson, P. Bjelkmar, R. Apostolov, M. R. Shirts, J. C. Smith, P. M. Kasson, D. van der Spoel, B. Hess, and E. Lindahl. (2013). "GROMACS 4.5: a high-throughput and highly parallel open source molecular simulation toolkit". *Bioinformatics.* **29** (7): 845-54. 10.1093/bioinformatics/btt055.

[28] J. Huang and A. D. MacKerell, Jr. (2013). "CHARMM36 all-atom additive protein force field: validation based on comparison to NMR data". *Journal of Computational Chemistry.* **34** (25): 2135-45. 10.1002/jcc.23354.

[29] L. Verlet. (1967). "Computer "Experiments" on Classical Fluids. I. Thermodynamical Properties of Lennard-Jones Molecules". *Physical Review.* **159** (1): 98-103. 10.1103/PhysRev.159.98.

[30] P. H. Hünenberger. (2005). In: "Advanced Computer Simulation, (Advances in Polymer Science, ch. Chapter 2". 105-149. 10.1007/b99427.

[31] R. Martonak, A. Laio, and M. Parrinello. (2003). "Predicting crystal structures: the Parrinello-Rahman method revisited". *Physical Review Letters.* **90** (7): 075503. 10.1103/PhysRevLett.90.075503.

[32] R. Kumari, R. Kumar, C. Open Source Drug Discovery, and A. Lynn. (2014). "g_mmpbsa --a GROMACS tool for high-throughput MM -PBSA calculations". *Journal of Chemical*

Information and Modeling. **54** (7): 1951-62. 10.1021/ci500020m.

[33] D. E. Pires, T. L. Blundell, and D. B. Ascher. (2015). "pkCSM: Predicting Small-Molecule Pharmacokinetic and Toxicity Properties Using Graph-Based Signatures". *Journal of Medicinal Chemistry.* **58** (9): 4066-72. 10.1021/acs.jmedchem.5b00104.

[34] A. Kunduracioglu. (2023). "A Computational (DFT) Study on the Anti-Malarial Drug: Lumefantrine". *Applied Sciences.* **13** (16). 10.3390/app13169219.

[35] K. El Khatabi, I. Aanouz, R. El-Mernissi, A. K. Singh, M. A. Ajana, T. Lakhlifi, S. Kumar, and M. Bouachrine. (2021). "Integrated 3D-QSAR, molecular docking, and molecular dynamics simulation studies on 1,2,3-triazole based derivatives for designing new acetylcholinesterase inhibitors". *Turkish Journal of Chemistry.* **45** (3): 647-660. 10.3906/kim-2010-34.

[36] H. Rasyid, N. Hariani Soekamto, Seniwati, S. Firdausiah, and Firdaus. (2023). "Modelling the Anticancer Activity of 4-Alkoxy Cinnamic Analogues using 3D-Descriptors and Genetic Algorithm-Multiple Linear Regression (GA-MLR) Method". *Journal of King Saud University - Science.* **35** (3). 10.1016/j.jksus.2022.102514.

[37] S. Y. Ho, K. Phua, L. Wong, and W. W. Bin Goh. (2020). "Extensions of the External Validation for Checking Learned Model Interpretability and Generalizability". *Patterns (NY).* **1** (8): 100129. 10.1016/j.patter.2020.100129.

[38] I. Miladiyah, J. Jumina, S. M. Haryana, and M. Mustofa. (2018). "Biological activity, quantitative structure-activity relationship analysis, and molecular docking of xanthone derivatives as anticancer drugs". *Drug Design, Development and Therapy.* **12** : 149-158. 10.2147/DDDT.S149973.

[39] H. Y. Guo, Z. A. Chen, Q. K. Shen, and Z. S. Quan. (2021). "Application of triazoles in the structural modification of natural products". *Journal of Enzyme Inhibition and Medicinal Chemistry.* **36** (1): 1115-1144. 10.1080/14756366.2021.1890066.

[40] T. A. Balogun, N. Ipinloju, O. T. Abdullateef, S. I. Moses, D. A. Omoboyowa, A. C. James, O. A. Saibu, W. F. Akinyemi, and E. A. Oni. (2021). "Computational Evaluation of Bioactive Compounds from Colocasia affinis Schott as a Novel EGFR Inhibitor for Cancer Treatment". *Cancer Informatics.* **20** : 11769351211049244. 10.1177/11769351211049244.

[41] O. Sawatdichaikul, S. Hannongbua, C. Sangma, P. Wolschann, and K. Choowongkomon. (2012). "In silico screening of epidermal growth factor receptor (EGFR) in the tyrosine kinase domain through a medicinal plant compound database". *Journal of Molecular Modeling.* **18** (3): 1241-54. 10.1007/s00894-011-1135-z.

[42] D. Ramirez and J. Caballero. (2018). "Is It Reliable to Take the Molecular Docking Top Scoring Position as the Best Solution without Considering Available Structural Data?". *Molecules.* **23** (5). 10.3390/molecules23051038.

[43] L. R. C. Suyo, J. P. Paulin, N. C. L. L. Gapaz, M. B. S. Arevalo, V. T. P. Yongco, and L. A. Santiago. (2024). "Molecular Docking, Pharmacological Profiling, and Molecular Dynamics Simulation of Potential Antihyperuricemic Agent from Secondary Metabolites of Dillenia philippinensis Rolfe (Dilleniaceae)". *Karbala International Journal of Modern Science.* **10** (3). 10.33640/2405-609x.3364.

[44] J. Ribas, E. Cubero, F. J. Luque, and M. Orozco. (2002). "Theoretical study of alkyl-pi and aryl-pi interactions. Reconciling theory and experiment". *Journal of Organic Chemistry.* **67** (20): 7057-65. 10.1021/jo0201225.

[45] S. Li, X. Zhou, W. Dong, M. Liu, W. Wang, Z. Zhao, L. Zhang, D. Yang, Y. Lu, and G. Du. (2025). "Regulating the physical and chemical properties of gefitinib and its positional isomer through salt formation". *Journal of Molecular Structure.* **1322**. 10.1016/j.molstruc.2024.140328.

[46] R. Wilcken, M. O. Zimmermann, A. Lange, A. C. Joerger, and F. M. Boeckler. (2013).

"Principles and applications of halogen bonding in medicinal chemistry and chemical biology". *Journal of Medicinal Chemistry.* **56** (4): 1363-88. 10.1021/jm3012068.

[47] P. Pandarangga, Y. Simarmata, A. B. H. Liu, and D. A. F. Haryati. (2024). "In silico simulation of hyperoside, isoquercetin, quercetin, and quercitrin as potential antivirals against the pNP868R protein of African swine fever virus". *Veterinary World.* **17** (1): 171-178. 10.14202/vetworld.2024.171-178.

[48] A. Hospital, J. R. Goni, M. Orozco, and J. L. Gelpi. (2015). "Molecular dynamics simulations: advances and applications". *Advances and Applications in Bioinformatics and Chemistry.* **8** 37-47. 10.2147/AABC.S70333.

[49] S. Roy, B. Maiti, N. Banerjee, M. H. Kaulage, K. Muniyappa, S. Chatterjee, and S. Bhattacharya. (2023). "New Xanthone Derivatives as Potent G-Quadruplex Binders for Developing Anti-Cancer Therapeutics". *ACS Pharmacol Transl Sci.* **6** (4): 546-566. 10.1021/acsptsci.2c00205.

[50] I. Sriyanti, D. Edikresnha, A. Rahma, M. M. Munir, H. Rachmawati, and K. Khairurrijal. (2017). "Correlation between Structures and Antioxidant Activities of Polyvinylpyrrolidone/Garcinia mangostana L. Extract Composite Nanofiber Mats Prepared Using Electrospinning". *Journal of Nanomaterials.* **2017** : 1-10. 10.1155/2017/9687896.

[51] I. H. Eissa, R. G.Yousef, H. Elkady, E. B. Elkaeed, A. A. Alsfouk, D. Z. Husein, I. M. Ibrahim, M. A. Asmaey, and A. M. Metwaly. (2023). "A new anticancer derivative of the natural alkaloid, theobromine, as an EGFR inhibitor and apoptosis inducer". *Theoretical Chemistry Accounts.* **143** (1). 10.1007/s00214-023-03071-z.

[52] S. Wan, R. Yan, Y. Jiang, Z. Li, J. Zhang, and X. Wu. (2019). "Insight into binding mechanisms of EGFR allosteric inhibitors using molecular dynamics simulations and free energy calculations". *The Journal of Biomolecular Structure and Dynamics.* **37** (16): 4384-4394. 10.1080/07391102.2018.1552197.

[53] Y. S. Kurniawan, E. Yudha, G. Nugraha, N. Fatmasari, H. D. Pranowo, J. Jumina, and E. N. Sholikhah. (2024). "Molecular Docking and Molecular Dynamic Investigations of Xanthone-Chalcone Derivatives against Epidermal Growth Factor Receptor for Preliminary Discovery of Novel Anticancer Agent". *Indonesian Journal of Chemistry.* **24** (1). 10.22146/ijc.88449.

[54] S. Alam and F. Khan. (2018). "Virtual screening, Docking, ADMET and System Pharmacology studies on Garcinia caged Xanthone derivatives for Anticancer activity". *Scientific Reports.* **8** (1): 5524. 10.1038/s41598-018-23768-7.

[55] C. A. Lipinski. (2004). "Lead- and drug-like compounds: the rule-of-five revolution". *Drug Discov Today Technol.* **1** (4): 337-41. 10.1016/j.ddtec.2004.11.007.

[56] A. Belkadi, S. Kenouche, N. Melkemi, I. Daoud, and R. Djebaili. (2022). "Molecular docking/dynamic simulations, MEP, ADME-TOX-based analysis of xanthone derivatives as CHK1 inhibitors". *Structural Chemistry.* **33** (3): 833-858. 10.1007/s11224-022-01898-z.